



CHORUS

This is the accepted manuscript made available via CHORUS. The article has been published as:

Room-Temperature Spin Polariton Diode Laser

Aniruddha Bhattacharya, Md Zunaid Baten, Ivan Iorsh, Thomas Frost, Alexey Kavokin, and
Pallab Bhattacharya

Phys. Rev. Lett. **119**, 067701 — Published 10 August 2017

DOI: [10.1103/PhysRevLett.119.067701](https://doi.org/10.1103/PhysRevLett.119.067701)

Room Temperature Spin Polariton Diode Laser

Aniruddha Bhattacharya,¹ Md Zunaid Baten,¹ Ivan Iorsh,^{2,3} Thomas Frost,¹ Alexey Kavokin,^{4,5,6} and Pallab Bhattacharya^{1*}

¹*Center for Photonics and Multiscale Nanomaterials,*

Department of Electrical Engineering and Computer Science, University of Michigan,

1301 Beal Avenue, Ann Arbor, Michigan 48109-2122, USA

²*National Research University for Information Technology, Mechanics and Optics (ITMO), St.*

Petersburg 197101, Russia

³*Division of Physics and Applied Physics, Nanyang Technological University 637371, Singapore*

⁴*School of Physics and Astronomy, University of Southampton, Southampton, SO17 1BJ,*

United Kingdom

⁵*Spin Optics Laboratory, State University of Saint-Petersburg, 1, Ulianovskaya, 198504, St.*

Petersburg, Russia

⁶*CNR-SPIN, Viale del Politecnico 1, I-00133, Rome, Italy*

*Electronic mail: pkb@umich.edu

A spin polarized laser offers inherent control of the output circular polarization. We have investigated the output polarization characteristics of a bulk GaN-based microcavity polariton diode laser at room temperature with electrical injection of spin polarized electrons via a FeCo/MgO spin injector. Polariton laser operation with a spin polarized current is characterized by a threshold of ~ 69 A/cm² in the light-current characteristics, a significant reduction of the electroluminescence linewidth and blueshift of the emission peak. A degree of output circular polarization of ~ 25 % is recorded under remanent magnetization. A second threshold, due to conventional photon lasing, is observed at an injection of ~ 7.2 kA/cm². The variation of output circular and linear polarization with spin-polarized injection current has been analyzed with the carrier and exciton rate equations and the Gross-Pitaevskii equations for the condensate and there is good agreement between measured and calculated data.

The output of a microcavity coherent light source is generally linearly polarized in the emitter-cavity photon strong coupling regime in the absence of pinning caused by photonic structural disorders [1-3]. However, it has been experimentally demonstrated that the orientation of this polarization is stochastic and hence the polarization cannot be experimentally recorded in the steady state [4, 5]. Linear polarization can be observed in the steady state output only by pinning along a preferred crystallographic axis [6-10] and the degree of polarization decreases at high pumping levels due to the depinning effect caused by polariton-polariton repulsive interactions and self-induced Larmor precession of the Stokes vector of the condensate [11]. These trends in the linear polarization have been observed in polariton lasers pumped optically [9] and electrically [10]. In the case of optical excitation, it is also possible to obtain a circularly polarized output above threshold and this behavior has been verified experimentally in the steady state at cryogenic temperatures [12-15]. The degree of circular polarization is determined by the interplay of polariton thermalization by scattering (polariton-phonon, polariton-electron and polariton-polariton) and polariton pseudospin precession in the effective magnetic field due to the TE-TM splitting [2, 16]. Circular polarization has not been observed in the output of an electrically injected polariton laser since carriers are injected with no net polarization [17]. The output can be circularly polarized due to the interplay of spin-dependent polariton-polariton interactions and stimulated relaxation of exciton polaritons at high injection densities where the depinning of linear polarization is observed [9], but this circular polarization is small, random and largely uncontrolled. On the other hand, it is possible to obtain a controlled and variable circularly polarized output by electrically injecting spin polarized carriers with a suitable ferromagnetic contact [20, 21] or a diluted magnetic semiconductor [22-24] acting as a spin

injector, as demonstrated with conventional photon lasers designed as vertical cavity surface-emitting lasers (VCSELs) [25-27] and light-emitting diodes (LEDs) [20-21, 28-29].

In the present study, we have investigated the output circular polarization characteristics of a polariton diode laser where spin polarized electrons are injected by a ferromagnetic tunnel injection contact. Such a device with controllable output circular polarization is useful for the study of fibrous proteins, collagens and asymmetric photochemical reactions which are sensitive to circularly polarized light. Information can be encoded onto both the intensity as well as the polarization of light in an optical communication system, thus effectively doubling the bandwidth of communication channels [27, 30]. There have been several reports of exciton-polariton spintronic switches [31, 32] and circularly polarized polariton lasers [5, 12-14, 33]. In particular, Amo et al. have demonstrated a non-local, all-optical exciton-polariton spin switch based on a pump and probe scheme in a semiconductor microcavity, wherein a localized trigger switches on a large pump area and thus controls the polarization of the full emission [31]. In all these previous reports, the devices have been optically excited and their operation was limited to cryogenic temperatures. We demonstrate here, for the first time, modulation of circular polarization of the output of a GaN-based polariton laser at room temperature by electrical injection of spin-polarized electrons using a FeCo/MgO tunnel spin injector contact.

We have characterized several identical electrically pumped bulk GaN-based microcavity polariton lasers fabricated from a single epitaxially grown heterostructure sample schematically shown in Fig. 1(a). Device fabrication is described in the Supplemental Material [34]. Two significant changes are incorporated in our previously reported [10, 35-37] polariton laser diodes to accomplish successful electrical spin injection and transport. First, the regular n-type ohmic contact is replaced by n-type FeCo/MgO spin-injector contacts to introduce a net electron spin

imbalance in the laser diode. The spin polarization of the injection current is dependent on the electron spin injection efficiency, for which a value of $\sim 8\%$ has been reported for the FeCo/MgO contact at room temperature [38]. Second, the diode heterostructure is grown on a p-type substrate so that the FeCo/MgO spin contact can be formed on the n-GaN layer on top. This reduces the transport length of the spin-polarized electrons to the active recombination region. The longitudinal spin transport length is ~ 400 nm in these devices, which is approximately twice that of the measured spin diffusion length at room temperature [38]. Since the microcavity diodes have an edge-emitting geometry, wherein the direction of cavity resonance and current injection are in mutually orthogonal directions, a parasitic contribution to the output circular polarization arising from magnetic circular dichroism (MCD) is absent in our diode lasers. The in-plane magnetization of FeCo enables the use of an edge-emitting geometry, which utilizes the important advantages of ferromagnetic metals such as small coercive fields and high remanent magnetization. These are the characteristics which allow nonvolatile spin manipulation using modest magnetic fields and is thus a very practical consideration for device applications. Further, the use of a bulk (three-dimensional) active layer ensures that the heavy-hole exciton pseudo-spin can, in principle, be oriented along the direction of light propagation, as the electron spin and the heavy-hole angular momenta can both be aligned along the edge. The device cross-section being small, any difference in the measured characteristics between the devices is attributed to the number of defects in the active region. The defect density in the active region is $\sim 6.1 \times 10^8 \text{ cm}^{-2}$ [37]. All measurements reported here have been done at room temperature. The microcavity quality factor, Q , and the corresponding cavity mode lifetime, τ_{ph} , are determined to be ~ 3200 and ~ 0.6 ps, respectively, from microphotoluminescence measurements. Angle-resolved electroluminescence measurements (Supplemental Material [34]) were made to

ascertain the strong coupling regime of operation of the devices and to determine the polariton dispersion characteristics. The measurements were carried out at a low value of continuous wave (CW) current injection, later confirmed to be $\sim 0.95 J_{\text{th}}$, where J_{th} is the non-linear threshold current density for polariton lasing. The data are shown in Fig. 1(b). From analysis of these data, in the framework of the 2×2 coupled harmonic oscillator model, the cavity-to-exciton detuning Δ and vacuum-field Rabi splitting Ω_{VRS} are found to be -7.5 meV and 36.1 meV, respectively. The dispersion curves are calculated with a measured exciton linewidth of ~ 6 meV. Additional sets of sub-threshold angle-resolved electroluminescence characteristics measured in two identical devices with ferromagnetic and non-magnetic contacts and corresponding polariton dispersion curves are shown in the Supplemental Material [34]. The Δ and Ω_{VRS} values for these devices are also very similar to the values quoted above.

The output light-current (L-I) characteristics of the devices were determined by recording the electroluminescence in the direction normal ($k_{\parallel} \sim 0$) to the Bragg mirrors as a function of continuous wave (CW) injection current. The measurements were made with the injection of spin-polarized electrons via the FeCo/MgO contact in a remanent magnetization state. As shown in Fig. 1(d) (for the device of Figs. 1 (a) and (b)), a non-linear threshold signaling the onset of stimulated scattering is observed at a current density of $J_{\text{th}} = 69$ A/cm² which is close to the value reported previously in similar devices [10, 35-37]. The corresponding lower-polariton (LP) density at the non-linear threshold is $\sim 1.02 \times 10^{16}$ cm⁻³, calculated with a measured excitonic lifetime of ~ 0.71 ns (see Supplemental Material [34]). Similar L-I characteristics for another device are shown in Fig. 2(a). With further increase of the injection current, the transition from strong to weak coupling takes place and a second non-linearity, most possibly due to population inversion and photon lasing, is observed at $J \sim 7.2$ kA/cm² (Fig. 2(b)). The threshold is shown

more clearly in the inset of this figure. The onset of non-linearity and polariton lasing threshold are accompanied by an abrupt reduction of the LP emission linewidth and a blue-shift of the LP electroluminescence peak energy (~ 9 meV at the polariton lasing threshold) shown in Fig. 2 (c). The minimum measured LP emission linewidth amongst all the devices measured is ~ 970 μeV , which corresponds to a LP coherence time of ~ 4 ps. The spontaneous radiative recombination lifetime of the lower polaritons in the condensate is estimated to be $\tau_{\text{LP}} = \tau_{\text{ph}} / |C(k_{\parallel} = 0)|^2 \sim 1.1$ ps. The polariton occupation in momentum space at different injection levels was also measured in the same device by angle-resolved electroluminescence in several devices. The occupation is calculated from the output power measured with an optical power meter. The polariton condensate occupation numbers are very similar in all the devices. Representative data are shown in Fig. 2 (d). A random and non-thermal LP occupation below threshold transforms to a peaked occupancy at $k_{\parallel} \sim 0$ above threshold, indicating the formation of a coherent bosonic condensate. It may be observed, from Fig. 2(d) that there is no appreciable saturation of the thermal part of the emitted LP intensity with injection beyond threshold. In general, for polariton lasers being operated in the kinetic regime, no such saturation should be expected [39]. Further, the population of certain excited states above the condensate may increase above the polariton lasing threshold due to the interplay of the phonon-assisted polariton scattering and polariton-polariton scattering. In the previous works on GaN-based polariton lasers, it has been observed that polariton-polariton interactions give rise to non-linear increase of the emission intensity with the pump intensity at large emission angles [40].

We measured the degree of circular polarization of the polariton emission in the normal direction ($k_{\parallel} \sim 0$) (see Supplemental Material [34]) as a function of injection current in multiple devices after the application of a suitable in-plane magnetizing field to the n-type FeCo/MgO

spin injector. The measurements were made in remanence with the magnetic field switched off. The degree of circular polarization above threshold follows the measured in-plane magnetization of a ~ 80 nm FeCo layer, which demonstrates that the observed electroluminescence polarization originates from the FeCo contact (see Supplemental Material [34]). Figure 3(a) shows the circular-polarization resolved LP electroluminescence intensities measured as a function of injection after magnetization of the contacts with $H \sim + 1.6$ kOe. Below the non-linear threshold, the degree of circular polarization of the microcavity emission is essentially zero because of complete spin relaxation of the excitons. Above the polariton lasing threshold, with the onset of stimulated LP-LP scattering, the dynamics which populate the LP condensate states become much faster than competing spin relaxation processes and one of the spin-polarized components of the condensate increases faster than the other giving rise to a net output circular polarization. Any possible difference in threshold between the two components might be small and within the limits of experimental error. Figure 3(b) depicts the measured steady state circular polarization of the output LP electroluminescence of the same device as a function of injection. There is a non-linear increase of the polarization at threshold and a maximum value of output circular polarization of ~ 25 % is observed above the non-linear threshold.

We have also measured the steady state linear polarization of the output LP electroluminescence as a function of the injected current density of the device whose L-I characteristics are depicted in Fig. 2(b) (see Supplemental Material [34]). The trend of the polarization is similar to what we have observed before with devices having non-magnetic contacts [10]. Below the non-linear threshold, the degree of linear polarization is below the detection limit of the measurement system. Above threshold, a maximum linear polarization of ~ 33 % is recorded for an injection level of ~ 72.5 A/cm². The linear polarization is found to be

preferentially oriented along the $[1\bar{1}00]$ crystallographic axis in all the devices. At threshold, there is a sharp increase in linear polarization due to the stimulated LP-LP scattering from the unpolarized reservoir to the polarized seed condensate in the presence of a small linear polarization splitting at $k_{\parallel} \sim 0$. This is followed by a peaking and a rapid decrease at higher injection due to the depinning effect [9, 11]. The measured threshold for linear polarization is in good agreement with the non-linear threshold in the light-current characteristics, within the limits of experimental accuracy.

The circular polarization is superimposed on the linear polarization of the output to produce a net elliptic polarization. We have analyzed the measured polarization results, with some simplifying assumptions, with the object of verifying the build-up of circular spin polarization due to the bosonic stimulation effect. We assume that the injected carriers are partially spin polarized. We also assume that the ground state of the polariton condensate is subject to the in-plane effective magnetic field originating from the splitting of X and Y polarized polariton states. The spin-dependent polariton-polariton interactions in the condensate are considered. Holes are assumed to be unpolarized and thus the spin polarization in the electron-hole plasma originates entirely due to the spin-polarized electrons. We solve the rate equations for free carriers and incoherent excitons as well as the Gross-Pitaevskii equations for the polariton condensate written in the basis of spin-up and spin-down electron states and corresponding optically active exciton states:

$$\begin{aligned}
\frac{dN_e^\uparrow}{dt} &= \xi P - W_{exc-form} N_e^\uparrow N_R^\uparrow + \frac{1}{\tau_{s,e}} (N_e^\downarrow - N_e^\uparrow); \quad \frac{dN_e^\downarrow}{dt} = (1-\xi)P - W_{exc-form} N_e^\downarrow N_R^\downarrow - \frac{1}{\tau_{s,e}} (N_e^\downarrow - N_e^\uparrow) \\
\frac{dN_R^{\uparrow,\downarrow}}{dt} &= -\frac{N_R^{\uparrow,\downarrow}}{\tau_R} + W_{exc-form} N_e^{\uparrow,\downarrow} N_R^{\uparrow,\downarrow} \pm \frac{1}{\tau_{s,R}} (N_R^{\downarrow,\downarrow} - N_R^{\uparrow,\uparrow}) - (a_{ph} N_R^{\uparrow,\downarrow} + b_{exc} N_R^{\uparrow,\downarrow 2}) (1 + |\Psi^{\uparrow,\downarrow}|^2) \\
i\hbar \frac{d\Psi^{\uparrow,\downarrow}}{dt} &= E\Psi^{\uparrow,\downarrow} + i\hbar(a_{ph} N_R^{\uparrow,\downarrow} + b_{exc} N_R^{\uparrow,\downarrow 2})\Psi^{\uparrow,\downarrow} - \frac{i\hbar}{\tau_c} \Psi^{\uparrow,\downarrow} + \alpha_1 |\Psi^{\uparrow,\downarrow}|^2 \Psi^{\uparrow,\downarrow} + \alpha_2 |\Psi^{\downarrow,\uparrow}|^2 \Psi^{\uparrow,\downarrow} \pm \Omega \Psi^{\downarrow,\uparrow}
\end{aligned}$$

(1)

Here $N_e^\uparrow, N_e^\downarrow, N_R^\uparrow, N_R^\downarrow$ are the electron and exciton reservoir occupation numbers corresponding to spin-up and spin-down electron states, respectively, $\Psi^\uparrow, \Psi^\downarrow$ are the wavefunctions of spin-up and spin-down polariton condensates, ξ is the degree of spin polarization of the injection current corresponding to an electron spin injection efficiency of $\sim 8\%$ [38], P is the injected current density; $W_{exc-form} \sim 0.1 \text{ ps}^{-1}$ is the exciton formation rate, $\tau_{s,e} \sim 40 \text{ ps}$ is the electron spin relaxation time [38], $\tau_{s,R} \sim 0.2 \text{ ps}$ is the exciton pseudospin relaxation time [41], $\tau_R = 1 \text{ ns}$ is the exciton non-radiative recombination time, $a_{ph} = 7 \times 10^{-10} \text{ ps}^{-1}$, $b_{exc} = 10^{-10} \text{ ps}^{-1}$ are the phonon-polariton and polariton-polariton scattering rates, $\tau_c \sim 1 \text{ ps}$ is the polariton lifetime, $\alpha_1 = 4 \mu\text{eV}, \alpha_2 = -0.4 \mu\text{eV}$ are the nonlinearity parameters describing the interactions of polaritons with parallel and antiparallel spins, respectively, and $\Omega = 0.1 \text{ meV}$ is the linear polarization splitting that governs the effective magnetic field acting upon the polariton pseudospin components [9]. The calculated variation of circular polarization with injection is shown alongside the measured data in Fig. 3(c) and a good agreement is observed. In contrast, calculations performed assuming the weak-coupling regime of operation (zero magnitudes for the interaction coefficients and the linear polarization splitting) cannot reproduce the measured

data. We conclude that stimulated scattering of spin-polarized excitons to the polariton condensate above the lasing threshold leads to the build-up of circular polarization of the emission of polariton lasers which paves the way to realization of a low-threshold semiconductor source of coherent circularly polarized UV to blue light. In contrast, spin-VCSELs have to be magnetized along the hard axis of the spin-injector and thus require higher fields for operation [25-27]. Further, while the operation of the spin polariton laser considered in the present study is at room temperature, spin-VCSELs have been operated only at low temperatures. The threshold current densities of previously reported electrically injected spin-VCSELs range from ~ 2 kA/cm² to ~ 8 kA/cm² [25, 26]. The threshold current densities in the present spin-polarized polariton lasers range from ~ 69 A/cm² to ~ 181 A/cm², which are significantly lower. While we observe a degree of output circular polarization of ~ 25 % in the present devices above threshold, a degree of circular polarization ranging from ~ 8 % [26] to ~ 23 % [25] were observed in the spin-VCSELs. Higher degrees of circular polarization (~ 55 %) were also demonstrated in the spin-VCSELs by adopting a specialized electrical biasing scheme [27].

In conclusion, we have demonstrated electrical spin injection from a FeCo/MgO Schottky tunnel barrier in an electrically pumped spin polariton diode laser. The polariton lasing characteristics have been measured with spin polarized injection current in remanence. The measured output circular and linear polarization have been analyzed by solving the rate equations for free carriers and excitons and the Gross-Pitaevskii equations for the polariton condensate. The device represents a bias-tunable low energy coherent polarized light source operating at room temperature.

Acknowledgements

The work is supported by the National Science Foundation under the Materials Research Science and Engineering Center (MRSEC) program (Grant No. DMR-1120923). Plasma-assisted molecular beam epitaxial growth of the devices and device processing were carried out in the Robert H. Lurie Nanofabrication Facility. I.I. acknowledges support of Grant No. MK-5220.2015.2 and from the Singaporean Ministry of Education under AcRF Tier 2 Grant No. MOE2015-T2-1-055. A.K. acknowledges support from the Engineering and Physical Sciences Research Council (EPSRC) Programme Grant No. EP/M025330/1 “Hybrid Polaritonics.”

References:

1. I. A. Shelykh, Yuri G. Rubo, G. Malpuech, D. D. Solnyshkov, and A. Kavokin, Phys. Rev. Lett. **97**, 066402 (2006).
2. F. P. Laussy, I. A. Shelykh, G. Malpuech, and A. Kavokin, Phys. Rev. B **73**, 035315 (2006).
3. G. Malpuech, M. M. Glazov, I. A. Shelykh, P. Bigenwald, and K. V. Kavokin, Appl. Phys. Lett. **88**, 111118 (2006).
4. J. J. Baumberg, A. V. Kavokin, S. Christopoulos, A. J. D. Grundy, R. Butté, G. Christmann, D. D. Solnyshkov, G. Malpuech, G. Baldassarri Höger von Högersthal, E. Feltin, J.-F. Carlin, and N. Grandjean, Phys. Rev. Lett. **101**, 136409 (2008).
5. H. Ohadi, E. Kammann, T. C. H. Liew, K. G. Lagoudakis, A. V. Kavokin, and P. G. Lagoudakis, Phys. Rev. Lett. **109**, 016404 (2012).
6. J. Kasprzak, M. Richard, S. Kundermann, A. Baas, P. Jeambrun, J. M. J. Keeling, F. M. Marchetti, M. H. Szymanska, R. Andre, J. L. Staehli, V. Savona, P. B. Littlewood, B. Deveaud, and L. S. Dang, Nature **443**, 409 (2006).

7. J. Kasprzak, R. André, Le Si Dang, I. A. Shelykh, A. V. Kavokin, Yuri G. Rubo, K. V. Kavokin, and G. Malpuech, *Phys. Rev. B* **75**, 045326 (2007).
8. R. Balili, V. Hartwell, D. Snoke, L. Pfeiffer, and K. West, *Science* **316**, 1007 (2007).
9. J. Levrat, R. Butté, T. Christian, M. Glauser, E. Feltin, J.-F. Carlin, N. Grandjean, D. Read, A. V. Kavokin, and Y. G. Rubo, *Phys. Rev. Lett.* **104**, 166402 (2010).
10. A. Bhattacharya, M. Z. Baten, I. Iorsh, T. Frost, A. Kavokin, and P. Bhattacharya, *Phys. Rev. B* **94**, 035203 (2016).
11. D. Read, T. C. H. Liew, Y. G. Rubo, and A. V. Kavokin, *Phys. Rev. B* **80**, 195309 (2009).
12. M. D. Martín, G. Aichmayr, L. Viña, and R. André, *Phys. Rev. Lett.* **89**, 077402 (2002).
13. H. Deng, G. Weihs, D. Snoke, J. Bloch, and Y. Yamamoto, *Proc. Natl. Acad. Sci.* **100**, 15318 (2003).
14. I. Shelykh, K. V. Kavokin, A. V. Kavokin, G. Malpuech, P. Bigenwald, H. Deng, G. Weihs, and Y. Yamamoto, *Phys. Rev. B* **70**, 035320 (2004).
15. K. V. Kavokin, I. A. Shelykh, A. V. Kavokin, G. Malpuech, and P. Bigenwald, *Phys. Rev. Lett.* **92**, 017401 (2004).
16. G. Panzarini, L. C. Andreani, A. Armitage, D. Baxter, M. S. Skolnick, V. N. Astratov, J. S. Roberts, A. V. Kavokin, M. R. Vladimirova, and M. A. Kaliteevski, *Phys. Rev. B* **59**, 5082 (1999).
17. The steady-state output circular polarization, observed in GaAs-based electrically injected polariton lasers (see, for example, Refs. [18] and [19]) operated with a high magnetic field ($B \sim 7$ T) in the Faraday geometry, originates from the Zeeman splitting

induced by the magnetic field and subsequent LP condensation in the less energetic of the two circularly- polarized LP ground states (for example, σ^+ -state in Ref. [18]).

18. P. Bhattacharya, B. Xiao, A. Das, S. Bhowmick, and J. Heo, Phys. Rev. Lett. **110**, 206403 (2013).
19. C. Schneider, A. Rahimi-Iman, N. Y. Kim, J. Fischer, I. G. Savenko, M. Amthor, M. Lerner, A. Wolf, L. Worschech, V. D. Kulakovskii, I. A. Shelykh, M. Kamp, S. Reitzenstein, A. Forchel, Y. Yamamoto, and S. Höfling, Nature (London) **497**, 348 (2013).
20. H. J. Zhu, M. Ramsteiner, H. Kostial, M. Wassermeier, H.-P. Schönherr, and K. H. Ploog, Phys. Rev. Lett. **87**, 016601 (2001); M. Ramsteiner, H. Y. Hao, A. Kawaharazuka, H. J. Zhu, M. Kästner, R. Hey, L. Däweritz, H. T. Grahn, and K. H. Ploog, Phys. Rev. B **66**, 081304(R) (2002); A. T. Hanbicki, B. T. Jonker, G. Itskos, G. Kioseoglou, and A. Petrou, Appl. Phys. Lett. **80**, 1240 (2002); A. T. Hanbicki, O. M. J. van 't Erve, R. Magno, G. Kioseoglou, C. H. Li, B. T. Jonker, G. Itskos, R. Mallory, M. Yasar, and A. Petrou, Appl. Phys. Lett. **82**, 4092 (2003).
21. V. F. Motsnyi, J. De Boeck, J. Das, W. Van Roy, G. Borghs, E. Goovaerts, and V. I. Safarov, Appl. Phys. Lett. **81**, 265 (2002); X. Jiang, R. Wang, R. M. Shelby, R. M. Macfarlane, S. R. Bank, J. S. Harris, and S. S. P. Parkin, Phys. Rev. Lett. **94**, 056601 (2005).
22. J. Carlos Egues, Phys. Rev. Lett. **80**, 4578 (1998).
23. D. Hägele, M. Oestreich, W. W. Rühle, N. Nestle, and K. Eberl, Appl. Phys. Lett. **73**, 1580 (1998).

24. M. Oestreich, J. Hübner, D. Hägele, P. J. Klar, W. Heimbrod, W. W. Rühle, D. E. Ashenford, and B. Lunn, *Appl. Phys. Lett.* **74**, 1251 (1999).
25. M. Holub, J. Shin, D. Saha, and P. Bhattacharya, *Phys. Rev. Lett.* **98**, 146603 (2007).
26. D. Basu, D. Saha, C. C. Wu, M. Holub, Z. Mi, and P. Bhattacharya, *Appl. Phys. Lett.* **92**, 091119 (2008); D. Basu, D. Saha, and P. Bhattacharya, *Phys. Rev. Lett.* **102**, 093904 (2009).
27. D. Saha, D. Basu, and P. Bhattacharya, *Phys. Rev. B* **82**, 205309 (2010).
28. R. Fiederling, M. Keim, G. Reuscher, W. Ossau, G. Schmidt, A. Waag, and L. W. Molenkamp, *Nature (London)* **402**, 787 (1999); Y. Ohno, D. K. Young, B. Beschoten, F. Matsukura, H. Ohno, and D. D. Awschalom, *Nature (London)* **402**, 790 (1999); O. M. J. van't Erve, G. Kioseoglou, A. T. Hanbicki, C. H. Li, and B. T. Jonker, *Appl. Phys. Lett.* **89**, 072505 (2006); D. Banerjee, R. Adari, S. Sankaranarayan, A. Kumar, S. Ganguly, R. W. Aldhaferi, M. A. Hussain, A. S. Balamesh and D. Saha, *Appl. Phys. Lett.* **103**, 242408 (2013).
29. A. Bhattacharya, M. Z. Baten, T. Frost, and P. Bhattacharya, *IEEE Photon. Technol. Lett.* **29**, 338 (2017).
30. D. Banerjee, R. Adari, M. Murthy, P. Suggisetti, S. Ganguly, and D. Saha, *J. Appl. Phys.* **109**, 07C317 (2011); N. C. Gerhardt, M. Y. Li, H. Jähme, H. Höpfner, T. Ackemann, and M. R. Hofmann, *Appl. Phys. Lett.* **99**, 151107 (2011).
31. A. Amo, T. C. H. Liew, C. Adrados, R. Houdré, E. Giacobino, A. V. Kavokin, and A. Bramati, *Nature Photon.* **4**, 361 (2010).
32. T. K. Paraïso, M. Wouters, Y. Léger, F. Morier-Genoud, and B. Deveaud-Plédran, *Nature Mater.* **9**, 655 (2010); A. Dreismann, H. Ohadi, Y. del Valle-Inclan Redondo, R. Balili,

- Y. G. Rubo, S. I. Tsintzos, G. Deligeorgis, Z. Hatzopoulos, P. G. Savvidis, and J. J. Baumberg, *Nature Mater.* **15**, 1074 (2016).
33. G. Roumpos, C. W. Lai, T. C. H. Liew, Y. G. Rubo, A. V. Kavokin, and Y. Yamamoto, *Phys. Rev. B* **79**, 195310 (2009); H. Ohadi, A. Dreismann, Y. G. Rubo, F. Pinsker, Y. del Valle-Inclan Redondo, S. I. Tsintzos, Z. Hatzopoulos, P. G. Savvidis, and J. J. Baumberg, *Phys. Rev. X* **5**, 031002 (2015).
34. See Supplementary Material, which includes Refs. [4, 10, 37], for a description of the epitaxial growth and device processing, time-resolved photoluminescence, angle-resolved electroluminescence, and interferometry measurements, calculation of the effective polariton temperature, steady-state linear polarization characteristics, light-current characteristics of Device 3, magnetizing-field dependent above-threshold circular polarization characteristics, magnetizing-field dependent light-current characteristics, and descriptions of the various measurements.
35. P. Bhattacharya, T. Frost, S. Deshpande, M. Z. Baten, A. Hazari, and A. Das, *Phys. Rev. Lett.* **112**, 236802 (2014).
36. M. Z. Baten, T. Frost, I. Iorsh, S. Deshpande, A. Kavokin, and P. Bhattacharya, *Sci. Rep.* **5**, 11915 (2015).
37. M. Z. Baten, A. Bhattacharya, T. Frost, I. Iorsh, A. Kavokin, and P. Bhattacharya, *Appl. Phys. Lett.* **108**, 041102 (2016).
38. A. Bhattacharya, M. Z. Baten, and P. Bhattacharya, *Appl. Phys. Lett.* **108**, 042406 (2016).
39. J. Levrat, R. Butté, E. Feltn, J. F. Carlin, N. Grandjean, D. Solnyshkov, and G. Malpuech, *Phys. Rev. B* **81**, 125305 (2010).

40. S. Christopoulos, G. Baldassarri Höger von Högersthal, A. J. D. Grundy, P. G. Lagoudakis, A. V. Kavokin, J. J. Baumberg, G. Christmann, R. Butté, E. Feltin, J.-F. Carlin, and N. Grandjean, *Phys. Rev. Lett.* **98**, 126405 (2007).
41. T. Kuroda, T. Yabushita, T. Kosuge, A. Tackeuchi, K. Taniguchi, T. Chinone, and N. Horio, *Appl. Phys. Lett.* **85**, 3116 (2004).

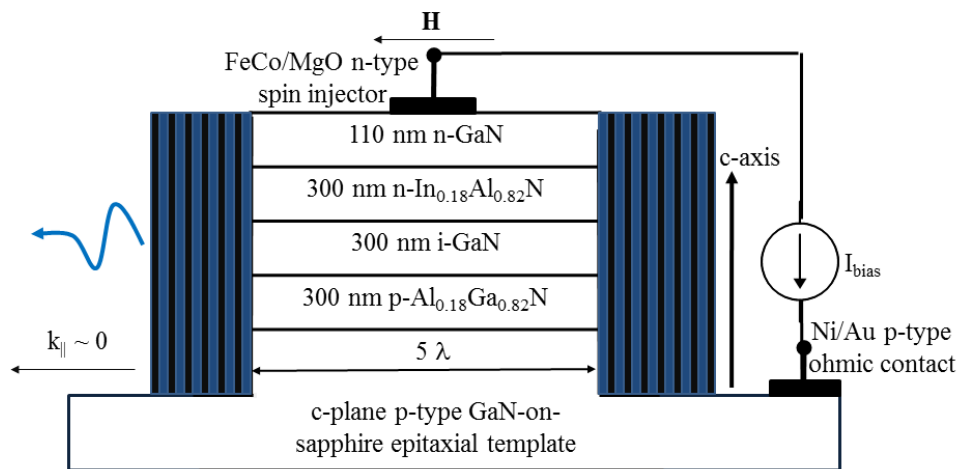
Figure Captions

Figure 1 (color online) (a) Schematic representation of the spin-polarized double heterostructure GaN-based microcavity diode (not drawn to scale) in the quasi-Voigt measurement geometry; (b) sub-threshold angle-resolved electroluminescence spectra recorded after in-plane magnetization of the ferromagnetic contacts with $H \sim + 1.6$ kOe. The spectra have been vertically offset for clarity. The dashed lines are guides to the eye representing the lower-polariton and excitonic transitions; (c) corresponding polariton dispersion curves calculated using a coupled harmonic oscillator model. The red (wine) circles represent the computed cavity photon (upper-polariton) dispersion and the blue circles correspond to the “data points” in (b); (d) normal incidence ($k_{\parallel} \sim 0$) LP electroluminescence intensities recorded as a function of injected current density after in-

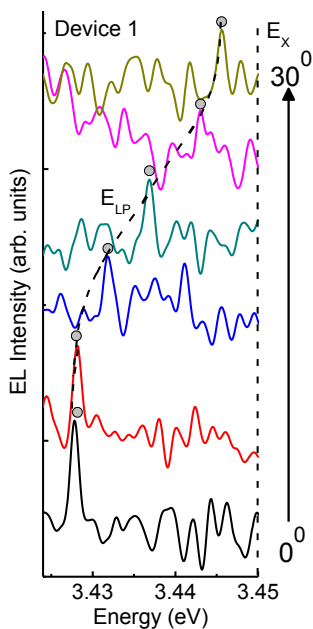
plane magnetization of the contacts with $H \sim \pm 1.6$ kOe. The vertical arrow indicates the onset of non-linearity.

Figure 2 (color online) (a) Normal incidence ($k_{\parallel} \sim 0$) LP electroluminescence intensities recorded as a function of injected current density; (b) two threshold lasing behavior with the nonlinearities due to polariton and photon lasing. The inset shows an enlargement highlighting the threshold at higher injection; (c) LP emission linewidth and blueshift of the LP electroluminescence peak emission energy as a function of injected current density. The resolution of the measurement (~ 4.6 meV) is indicated as a horizontal dashed line; (d) LP emission intensities for different k_{\parallel} states as a function of the energy difference $E(k_{\parallel}) - E(k_{\parallel} \sim 0)$, determined from angle-resolved electroluminescence measurements at different injection densities. The measurements were made after in-plane magnetization of ferromagnetic contacts with $H \sim + 1.6$ kOe. The vertical arrows in (a) and (b) indicate the onset of the non-linearity due to polariton lasing. The solid lines are guides to the eye.

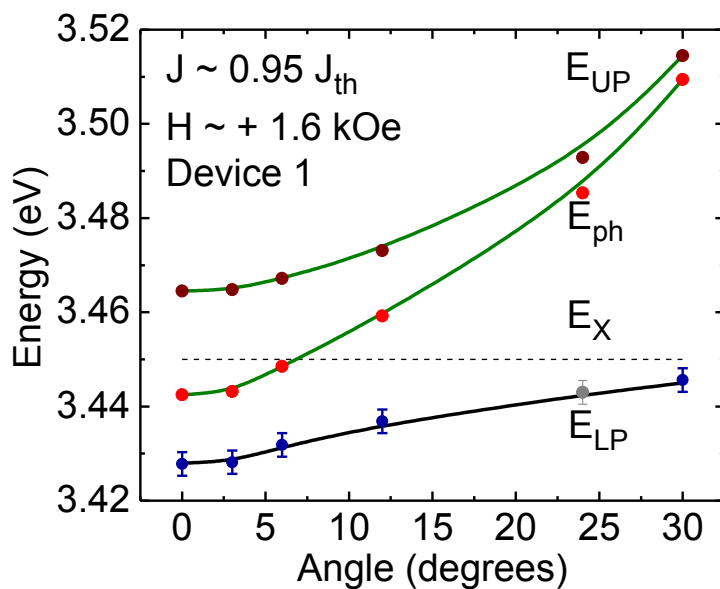
Figure 3 (color online) (a) Measured normal incidence ($k_{\parallel} \sim 0$) circular polarization-resolved LP electroluminescence intensities as a function of injected current density recorded after in-plane magnetization of ferromagnetic contacts with $H \sim + 1.6$ kOe. The total light intensity S is the summation of the right-hand (S^+) and left-hand circularly polarized (S^-) LP emission intensities. The arrow indicates the onset of non-linearity and the solid lines are guides to the eye; (b) measured steady-state degree of circular polarization as a function of injected current density recorded after in-plane magnetization of ferromagnetic contacts with $H \sim + 1.6$ kOe. The red (green) solid lines in (b) represent the calculated values assuming strong(weak)-coupling in the microcavity.



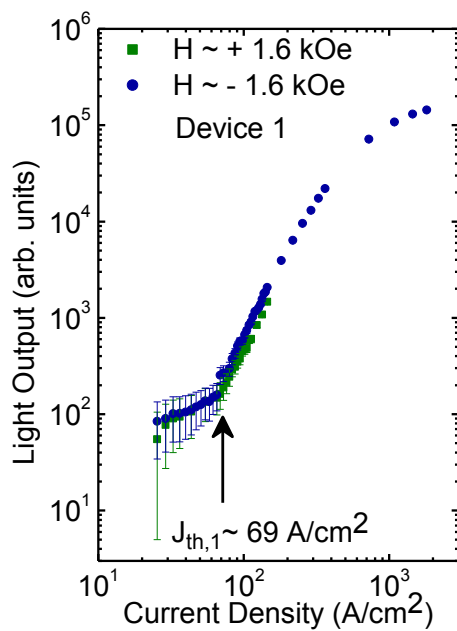
(a)



(b)



(c)



(d)

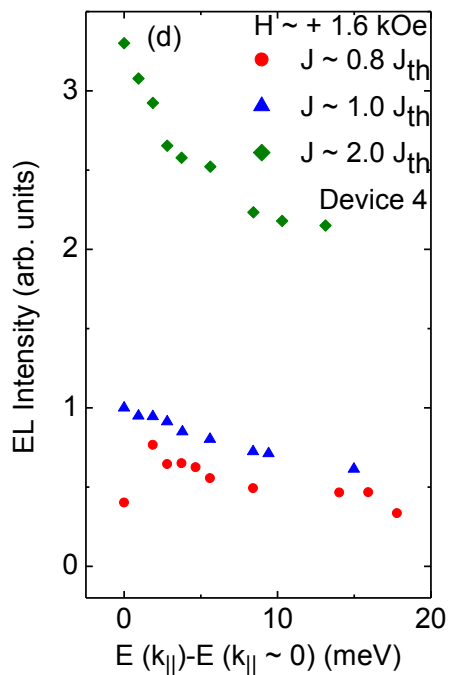
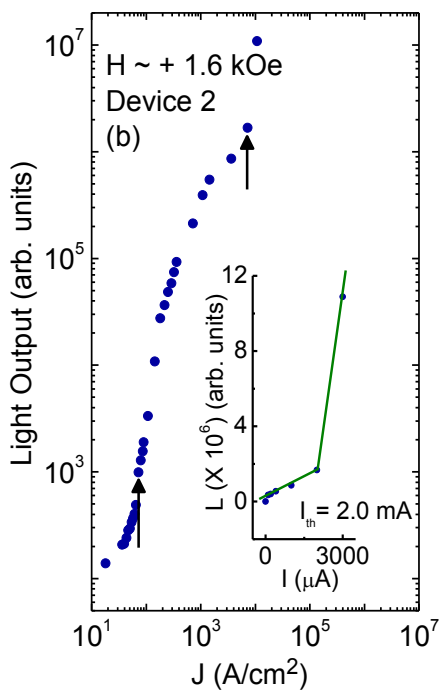
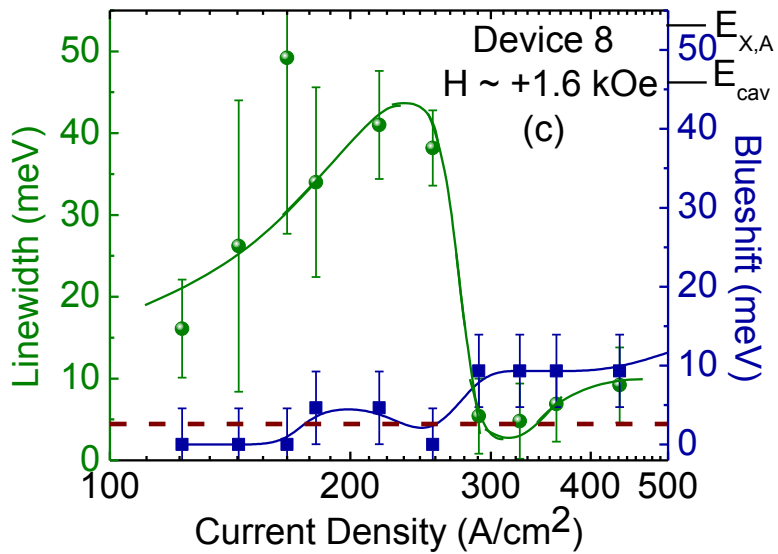
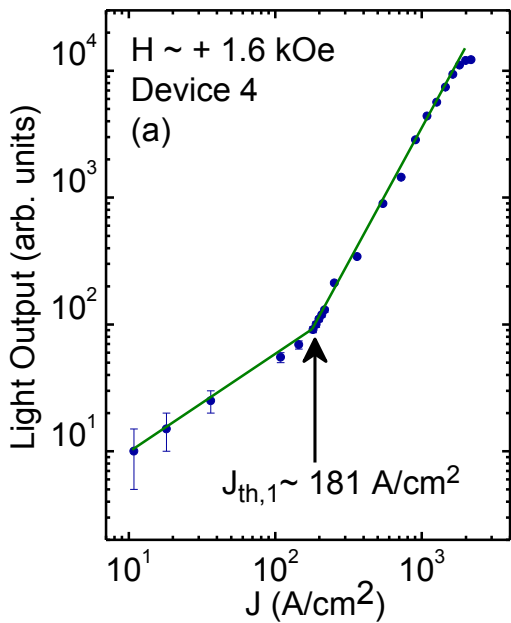
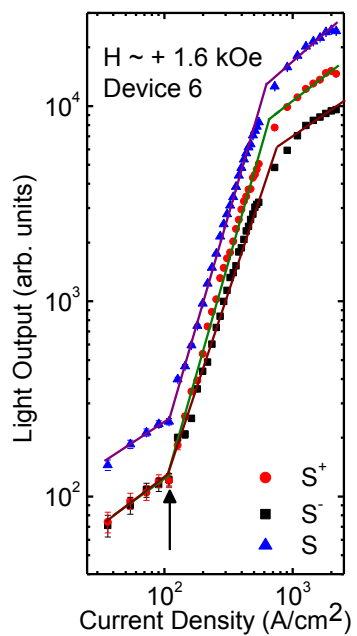
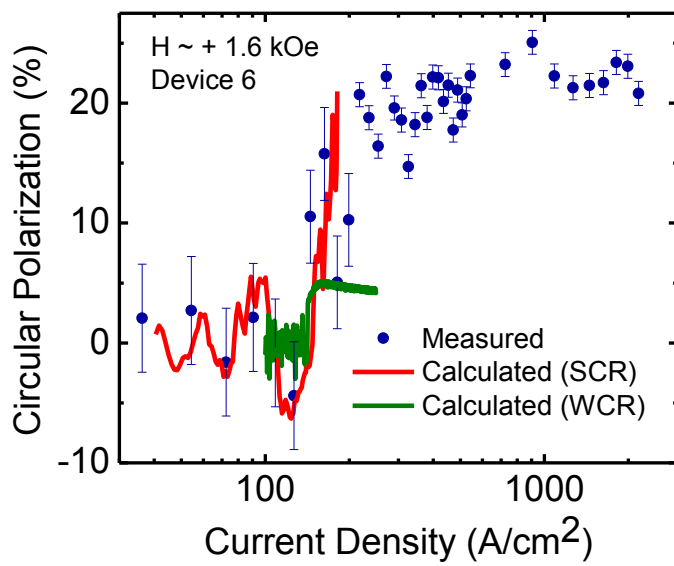


Figure 2 of 3



(a)



(b)